

LETTER • OPEN ACCESS

Atmospheric methane underestimated in future climate projections

To cite this article: Thomas Kleinen *et al* 2021 *Environ. Res. Lett.* **16** 094006

View the [article online](#) for updates and enhancements.

ENVIRONMENTAL RESEARCH
LETTERS

LETTER

Atmospheric methane underestimated in future climate projections

OPEN ACCESS

RECEIVED

23 March 2021

REVISED

6 July 2021

ACCEPTED FOR PUBLICATION

27 July 2021

PUBLISHED

12 August 2021

Thomas Kleinen^{1,*} , Sergey Gromov² , Benedikt Steil²  and Victor Brovkin¹ ¹ Max Planck Institute for Meteorology, Bundesstr. 53, 20146 Hamburg, Germany² Max Planck Institute for Chemistry, Hahn-Meitner-Weg 1, 55128 Mainz, Germany

* Author to whom any correspondence should be addressed.

E-mail: thomas.kleinen@mpimet.mpg.de**Keywords:** future climate, atmospheric methane, methane emissions, methane concentration

Original Content from this work may be used under the terms of the [Creative Commons Attribution 4.0 licence](https://creativecommons.org/licenses/by/4.0/).

Any further distribution of this work must maintain attribution to the author(s) and the title of the work, journal citation and DOI.

**Abstract**

Methane (CH₄) is the second most important naturally occurring greenhouse gas (GHG) after carbon dioxide (Myhre G *et al* 2013 *Climate Change 2013: The Physical Science Basis. Contribution of Working Group I to the Fifth Assessment Report of the Intergovernmental Panel on Climate Change* (Cambridge: Cambridge University Press) pp 659–740). For both GHGs, the present-day budget is dominated by anthropogenic emissions (Friedlingstein P *et al* 2019 *Earth Syst. Sci. Data* **11** 1783–838; Saunio M *et al* 2020 *Earth Syst. Sci. Data* **12** 1561–623). For CO₂ it is well established that the projected future rise in atmospheric concentration is near exclusively determined by anthropogenic emissions (Ciais P *et al* 2013 *Climate Change 2013: The Physical Science Basis. Contribution of Working Group I to the Fifth Assessment Report of the Inter-governmental Panel on Climate Change* (Cambridge: Cambridge University Press) pp 465–570). For methane, this appears to be the common assumption, too, but whether this assumption is true has never been shown conclusively. Here, we investigate the evolution of atmospheric methane until 3000 CE under five Shared Socioeconomic Pathway (SSP) scenarios, for the first time using a methane-enabled state-of-the-art Earth System Model (ESM). We find that natural methane emissions, i.e. methane emissions from the biosphere, rise strongly as a reaction to climate warming, thus leading to atmospheric methane concentrations substantially higher than assumed in the scenarios used for CMIP6. We also find that the natural emissions become larger than the anthropogenic ones in most scenarios, showing that natural emissions cannot be neglected.

1. Introduction

Projections of future climate are strongly dependent on the assumed concentrations of greenhouse gases (GHG). The GHG concentration scenarios used in Phase 6 of the Coupled Model Intercomparison Project (CMIP6) (O'Neill *et al* 2016) were derived using the reduced-complexity carbon cycle climate model MAGICC (Meinshausen *et al* 2011). One of the assumptions going into the determination of future methane concentrations is that the natural CH₄ emissions can be derived by closing the methane budget over a part of the historical period, in the case of the CMIP6 scenarios over the period 1994–2004 (Meinshausen *et al* 2020). These natural emissions are then assumed to remain constant over

the future period investigated. The approach thus relies on the assumption that changes in the natural emissions of methane are substantially less important than the anthropogenic emissions, an assumption that generally holds for carbon dioxide and was reasonable to make considering the published literature on future methane emissions at the time the MAGICC model was first published. In the light of the experiments presented here, however, this assumption will need to be reconsidered.

In the present-day top-down methane budget (Saunio *et al* 2020), about 40% of the methane emissions are attributed to natural sources, with wetland emissions being by far the largest component of the natural emissions. Measurements indicate that CH₄ emissions may increase under future climatic

conditions, from soils (van Groenigen *et al* 2011) as well as from several other natural methane sources (Dean *et al* 2018). Using a data-driven modelling approach, Koffi *et al* (2020) thus find an increase in natural emissions by 50%–80% by 2100. However, the future natural emissions of methane have only rarely been investigated in scenario experiments with ESMs to this date, likely because methane emissions are not yet a standard output of ESMs and require dedicated submodels. Shindell *et al* (2013) investigated future methane with a focus on atmospheric chemistry and found an increase of wetland emissions by 20% under RCP 8.5 until 2100. Denisov *et al* (2013), on the other hand, see an increase by 47% in natural emissions by 2100 under RCP 8.5. Finally, Zhang *et al* (2017), using a stand-alone land model, driven by climate scenarios from several climate models, find increases by up to 97% in wetland emissions. So far, no ESM study investigated future CH₄ concentrations beyond 2100 CE, although it is clear that future warming will persist for far longer, especially in the case of scenarios with high radiative forcing. Furthermore, previous studies mainly focused on single forcing factors.

Thus the objective of this study is twofold. First, we aim to extend the assessment of the consequences of future warming for the methane cycle beyond the time horizon investigated in previous studies, 2100 CE, using a state-of-the-art ESM, the Max Planck Institute for Meteorology Earth System Model (Mauritsen *et al* 2019) (MPI-ESM). Second, we assess the entirety of methane emission fluxes in a full methane cycle representation in order to determine the relative importance of both natural and anthropogenic forcings under five different climate change scenarios.

2. Methods

2.1. Methane emissions in MPI-ESM

We use MPI-ESM, the Max Planck Institute for Meteorology Earth System Model (Mikolajewicz *et al* 2018, Mauritsen *et al* 2019), consisting of the atmospheric general circulation model ECHAM6, the ocean general circulation model MPIOM, and the land surface model JSBACH in coarse resolution (T31GR30 $\approx 3.75^\circ \times 3.75^\circ$) to investigate the future evolution of the climate system and methane cycle for the next millennium. We have developed a methane-enabled version of MPI-ESM for paleoclimate applications. As described in Kleinen *et al* (2020), we use a TOPMODEL (Beven and Kirkby 1979) approach to determine inundated areas, in which we determine wetland methane emissions based on Riley *et al* (2011). Methane emissions from wildfires and biomass burning are determined from the SPITFIRE fire model (Lasslop *et al* 2014), using emission factors from Kaiser *et al* (2012). Termite methane emissions

are determined using the approach from Kirschke *et al* (2013) and Sauniois *et al* (2016).

In the TOPMODEL approach, the soil water content determined in the MPI-ESM land surface model JSBACH is combined with sub-gridscale topographic information, the Compound Topographic Index (CTI), in order to determine the variation of the water table in each model grid cell. We then use this to determine inundation fraction, the fraction of each grid cell where the water table is at or above the surface. In Kleinen *et al* (2020) we have evaluated the model for present-day climatic conditions against remote-sensing data of inundation (Prigent *et al* 2012) and found a reasonable agreement between model and data, considering the limitations of both model and remote-sensing data. Total extent and seasonality are rather similar for the NH extratropics, while the model slightly overestimates the extent for tropical wetlands.

We assume that soil carbon decomposition, described in JSBACH by the YASSO model (Goll *et al* 2015), occurs anaerobically in inundated areas, with YASSO rate constants reduced to 35% of the standard (aerobic) decomposition rates (Wania *et al* 2010). The anaerobically decomposed carbon results in production of CO₂ and CH₄, with a temperature-dependent partitioning of the anaerobic decomposition product into CO₂ and CH₄, as described by Riley *et al* (2011). Soil transport of O₂, CO₂ and CH₄ is determined in an emission model based on Riley *et al* (2011), which explicitly simulates methane transport via the pathways diffusion, ebullition, and plant aerenchyma, as well as the oxidation of CH₄, if sufficient oxygen is present. As CH₄ also diffuses into the soil in dry areas, where it is oxidised, the model also determines the soil sink of methane.

We do not model the CH₄ emissions from inland waters (lakes) explicitly, but rather assume that their emissions are implicitly contained in the wetland emission flux. This is a simplification made for practical reasons, as no appropriate model exists in the literature at present. We assume, however, that the error introduced by this simplification is relatively small on the scales the model was designed for ($\sim 350+$ km spatial resolution, decadal to centennial temporal scale). This assumption is based on two factors: the surface water extent data used to calibrate the wetland model also contains inland water bodies, and we assume that the changes in methane fluxes from inland waters on these scales will be driven by the same factors that drive the changes in wetland emissions, i.e. carbon, temperature, and precipitation. On shorter time (monthly to annual) and spatial (10s of kilometers) scales, the errors introduced through this simplification may be substantial, though.

Methane emissions from wildfires and biomass burning (with the sum subsequently called the ‘fire’ emissions) are determined from the SPITFIRE fire

model (Lasslop *et al* 2014), using emission factors from Kaiser *et al* (2012). The SPITFIRE fire model determines the spread of fires using the fire ignition probability, a function of lightning frequency and population density, and flammability (higher under dryer/warmer conditions), as well as the amount of biomass available for burning. The methane emissions are then determined from the burned biomass using emission factors. Termite methane emissions are determined using the approach from Kirschke *et al* (2013) and Saunois *et al* (2016), which determines termite mass from gross primary productivity in tropical areas and assumes a constant emission factor to determine the final methane emissions. Geological emissions are prescribed with a spatial distribution from Etiope (2015), but scaled to give a total of $5 \text{ TgCH}_4 \text{ yr}^{-1}$, based on Hmiel *et al* (2020).

In Kleinen *et al* (2020) we evaluated the modelled methane emissions for present-day (PD) climate. As flux measurements on appropriate scales are not available, we compared aggregate fluxes against global assessments (Saunois *et al* 2016). We found that the model simulates wetland methane emissions of $222 \text{ TgCH}_4 \text{ yr}^{-1}$ (decadal mean over 2000–2009), fire emissions of $17.6 \text{ TgCH}_4 \text{ yr}^{-1}$, termite emissions of $11.7 \text{ TgCH}_4 \text{ yr}^{-1}$, and a soil uptake of $17.5 \text{ TgCH}_4 \text{ yr}^{-1}$. These values fall well within the ranges reported by Saunois *et al* (2016), who report $153\text{--}227 \text{ TgCH}_4 \text{ yr}^{-1}$ for natural wetlands, $15\text{--}20 \text{ TgCH}_4 \text{ yr}^{-1}$ for biomass burning, $1\text{--}5 \text{ TgCH}_4 \text{ yr}^{-1}$ for wildfires, $3\text{--}15 \text{ TgCH}_4 \text{ yr}^{-1}$ for termites, and $9\text{--}47 \text{ TgCH}_4 \text{ yr}^{-1}$ for the soil uptake. Spatial patterns of PD emissions are also similar to those shown by Saunois *et al* (2016). Furthermore, wetland methane emission estimates from atmospheric inversions (Bousquet *et al* 2011) show that the majority (62%–77%) of the present-day emissions come from regions between 30° S and 30° N , while a much smaller part (20%–33%) are emitted from north of 30° N . Of the modelled total wetland CH_4 emissions for PD conditions, 70% are from low latitude regions, while 29% are from regions north of 30° N . The latitudinal distribution of modelled PD wetland methane emissions therefore is well within the range obtained from atmospheric inversions.

2.2. Atmospheric methane sink

The spatiotemporal evolution of methane abundance is simulated using a methane tracer undergoing transport, emission and chemical destruction in the atmospheric model ECHAM6. The CH_4 atmospheric sink is calculated using a zonally averaged methane reactivity field obtained from the comprehensive ECHAM/MESy Atmospheric Chemistry Model (EMAC) (Joeckel *et al* 2010). The tropospheric reactivity contribution is parameterised to account for changes in atmospheric oxidative capacity as follows (Gromov *et al* 2018):

$$r_{\text{CH}_4} = \alpha \times (LN + k_N RN)^p \times (M + k_C RC)^q (\text{yr}^{-1}), \quad (1)$$

with LN being the global lightning nitrogen oxides (NO_x) emission, simulated interactively according to Grewe *et al* (2001), M the CH_4 atmospheric burden, RN and RC the terrestrial (surface) emissions of reactive nitrogen and carbon compounds. All terms are given in TgC or TgN , respectively, per yr for the emission fluxes. Fit parameters ($\alpha = 2.74$, $p = 0.36$, $q = -0.48$, $k_N = 0.18$, $k_C = 3.10$) are obtained from an ensemble of EMAC simulations covering a wide range of RN , RC , LN and M values probed in last glacial maximum (LGM) and present-day conditions. The fitted r_{CH_4} value is accurate within (1.6–5.5)% at 95% CI. In the MPI-ESM experiments, the natural emission components of RN and RC are obtained from the MEGAN model (Guenther *et al* 2012) for the biogenic sources and from the SPITFIRE model (Lasslop *et al* 2014) with emission factors from Kaiser *et al* (2012) for biomass burning. We are using NO_x emissions (scaled by a factor of 2.5 to account for other N-containing compounds) as a proxy for the total natural RN term. For the RC term, CO and isoprene (C_5H_8), scaled by a factor of 1.4 to account for secondary biogenic co-emitted compounds, are used as proxies for the RC term. These scaling factors were derived by comparing the PD emissions of NO_x as well as CO and C_5H_8 with present-day RN and RC emissions. Where available, anthropogenic emissions of RC and RN are considered, as detailed below.

2.3. Model forcing

The model is forced with prescribed CO_2 and N_2O concentrations, as well as anthropogenic emissions of methane, NO_x , CO, and volatile organic compounds (VOC). We prescribed CO_2 concentrations from Meinshausen *et al* (2020) until 2500 (Meinshausen and Vogel 2016, Meinshausen and Nicholls 2018a, 2018b, 2018c, 2018d, 2018e). For the years 2501–3000 CE, CO_2 was calculated by the climate-carbon cycle model of intermediate complexity CLIMBER-2, used for glacial and interglacial simulations (Brovkin *et al* 2012, Kleinen *et al* 2016), assuming no additional anthropogenic CO_2 emissions or land use change. CLIMBER-2 accounts for the biogeochemical processes essential on multi-centennial timescales in the ocean (carbonate sedimentation) and on land (weathering, vegetation dynamics). N_2O concentrations were prescribed from Meinshausen *et al* (2020) until 2500 (Meinshausen and Vogel 2016, Meinshausen and Nicholls 2018a, 2018b, 2018c, 2018d, 2018e) and kept constant for 2501–3000 CE. The atmospheric CH_4 concentration was not prescribed, but rather modelled interactively from the methane sources and sinks calculated by MPI-ESM as described above.

Anthropogenic methane emissions for the historical period are available from Hoesly *et al* (2017a, 2018). While the data for 1970–2014 are part of the released input files for CMIP6, emissions for 1850–1969 are only available as supplementary data with higher uncertainty (Hoesly *et al* 2017b), and no anthropogenic CH₄ emissions for the time before 1850 have been published that are compatible with the Hoesly *et al* (2018) data set. The emissions before 1850, used in the model spinup, were thus interpolated linearly between 1770 and 1849, assuming zero anthropogenic emissions in 1770. This latter assumption is known to be wrong—agricultural emissions were certainly larger than zero before 1850—but as the atmospheric lifetime of methane is of the order of a decade, we assume that this slight underestimate is not relevant for later times.

Anthropogenic CH₄ emissions for 2015–2100 were prescribed from Gidden *et al* (2019) for the SSP scenarios (Gidden *et al* 2018a, 2018b, 2018c, 2018d, 2018e). For the time after 2100 we use the same approach as Meinshausen *et al* (2020): we assume that anthropogenic emissions from non-agricultural sources decline to zero over 150 years, while agricultural emissions stay constant at the 2100 CE level (figure 3). Similarly, anthropogenic emissions of NO_x, CO, and volatile organic compounds (VOC) were obtained from Hoesly *et al* (2017a, 2018) for the historical period, and from Gidden *et al* (2018a, 2018b, 2018c, 2018d, 2018e, 2019) for the SSP scenarios. These were interpolated linearly between 1650 and 1750, as well as between 2100 and 2250, assuming zero emissions in 1650 and 2250. We prescribed these as the anthropogenic shares of RC and RN emissions, with RC given by the sum of CO and VOC emissions, and RN given by the NO_x emissions, again scaled to match RN inventories.

Due to the nature of the model set-up, intended for paleoclimate simulations, we neglect two short-term climate forcings: anthropogenic emissions of aerosols and anthropogenic land use changes. The result of the former is that the model does not reflect the slight cooling trend, relative to the GHG-induced warming, induced by the aerosol loading during the 20th century. The effect of the latter is that the biogeophysical feedbacks between land surface and atmosphere are biased towards a natural system, i.e. high latitude temperatures are slightly warmer than they would be with land use, while tropical temperatures are slightly cooler. We judge the effect of this omission on CH₄ emissions to be minor. The primary effects of land-use on greenhouse gases are considered by prescribing atmospheric CO₂ concentrations, as well as anthropogenic CH₄ emissions, which contain the agricultural fluxes.

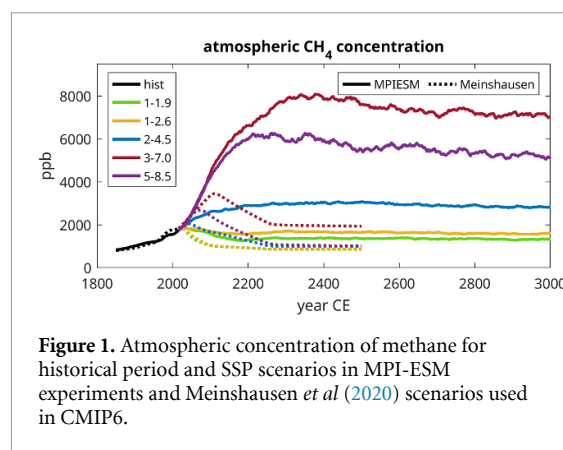


Figure 1. Atmospheric concentration of methane for historical period and SSP scenarios in MPI-ESM experiments and Meinshausen *et al* (2020) scenarios used in CMIP6.

2.4. Model experiments

We conduct a set of 5 model experiments, following the SSP scenarios 1–1.9, 1–2.6, 2–4.5, 3–7.0 and 5–8.5. All experiments are initialised for the year 1850 CE from an identical model state, and forcings for historical and future climate states are prescribed as described above.

We obtained the initial model state from a transient model experiment from the last glacial maximum (LGM) to the present, to be described in detail in a subsequent publication. Briefly, the transient experiment consisted of a spinup phase for several millennia at 26 ka BP boundary conditions, followed by a transient model integration for 26 000 model years. The model was forced by orbital changes from Berger (1978), atmospheric greenhouse gas concentrations from Köhler *et al* (2017), and the GLAC-1D ice sheet reconstruction (Tarasov *et al* 2012, Briggs *et al* 2014, Ivanovic *et al* 2016). We branched from this model experiment in the model year corresponding to 1550 CE, running it to 1850 CE with the full set of anthropogenic forcings as described above.

3. Results

3.1. Atmospheric CH₄ concentration in response to natural CH₄ emissions

In all scenarios investigated, the atmospheric global mean near-surface CH₄ concentrations in the model experiments (figure 1) are higher than in the published CMIP6 scenarios (Meinshausen *et al* 2020). In the case of the low radiative forcing scenarios SSP1–1.9 and SSP1–2.6, the concentration maximum occurs at the end of the historical period and does not differ significantly between our experiments and the published scenarios. The concentration decline after that maximum, however, occurs much more slowly in our experiments, leading to higher atmospheric methane concentrations than in the published scenarios. For the moderate to high warming scenarios

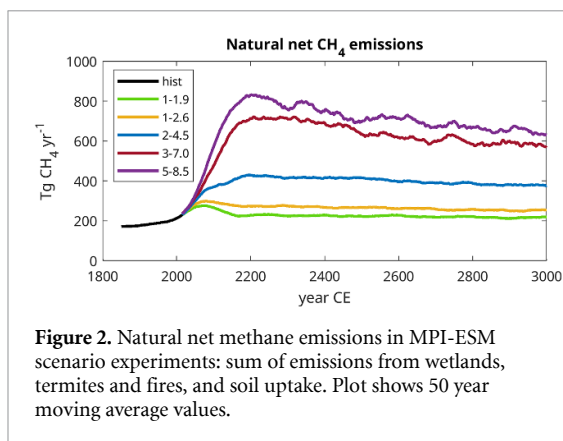


Figure 2. Natural net methane emissions in MPI-ESM scenario experiments: sum of emissions from wetlands, termites and fires, and soil uptake. Plot shows 50 year moving average values.

SSP2–4.5, SSP3–7.0 and SSP5–8.5, however, the evolution of atmospheric methane is much more dramatic. Here, maximum atmospheric concentrations become substantially higher than in the published scenarios and stay at a very high level until the end of the experiments in 3000 CE. For SSP2–4.5, the maximum in CH_4 is 50% higher than published previously, for SSP3–7.0 it is 131% higher and for SSP5–8.5 it is 130% higher. The maxima also occur substantially later, ~ 200 years in the case of SSPs 3–7.0 and 5–8.5, while it is 450 years in the case of SSP 2–4.5. Furthermore, the atmospheric concentrations given for the CMIP6 scenarios decrease relatively quickly after reaching their maxima, stabilising in 2250 CE, when the non-agricultural emissions cease in the Meinshausen *et al* (2020) scenarios. In our experiments, however, they remain high and decline much slower. This is due to the fact that the natural emissions increase with warming in our model, while Meinshausen *et al* assume constant PD emissions. As a consequence, radiative forcing by methane also increases. Following Etminan *et al* (2016), the methane radiative forcing change from preindustrial is 0.64 Wm^{-2} for 2010 CE. Assuming SSP 3–7.0, it increases to 1.31 Wm^{-2} in 2110 when following the GHG scenario from Meinshausen *et al* (2020). Using our model results, however, it peaks at 2.37 Wm^{-2} in 2377 to -81% larger than following the published scenario (figure A3).

The reason for these high concentrations of atmospheric methane is that the natural emissions of CH_4 are substantially higher than assumed previously. While Meinshausen *et al* (2020) assumed that the natural emissions would stay constant, they rise roughly proportionally to temperature change in our model experiments (figure 2).

Mean natural net CH_4 emissions, i.e. the sum of emissions from wetlands, termites, fires, and the soil methane uptake, for 2000–2009 are $220 \text{ TgCH}_4 \text{ yr}^{-1}$, and emissions increase by between 22% and 149% in 2100 CE (table 1), becoming larger than the 2000–2009 mean in all scenario experiments. Furthermore, net natural emissions keep increasing

Table 1. SSP scenario experiment natural CH_4 emissions (E) in 2100 (mean 2090–2099), maximum decadal mean natural CH_4 E and decade of maximum in scenario experiments, maximum anthropogenic CH_4 E and year of maximum. Emissions in $\text{TgCH}_4 \text{ yr}^{-1}$.

Scenario	Nat. E 2100	Max. nat. E (decade)	Max. anth. E (year)
1–1.9	269	276 (2070)	379 (2016)
1–2.6	296	299 (2070)	379 (2016)
2–4.5	368	430 (2190)	390 (2031)
3–7.0	460	719 (2310)	757 (2100)
5–8.5	548	831 (2200)	588 (2061)

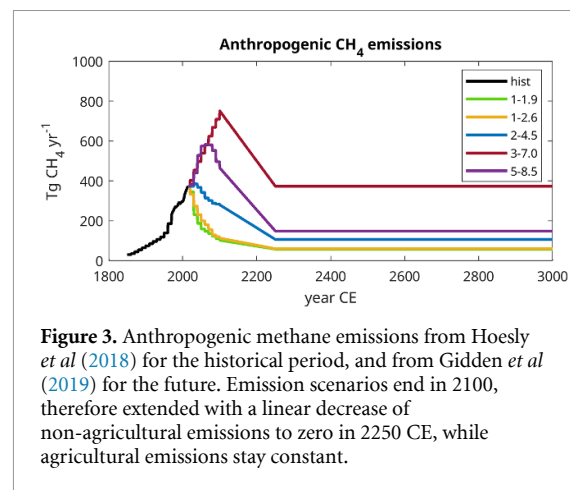
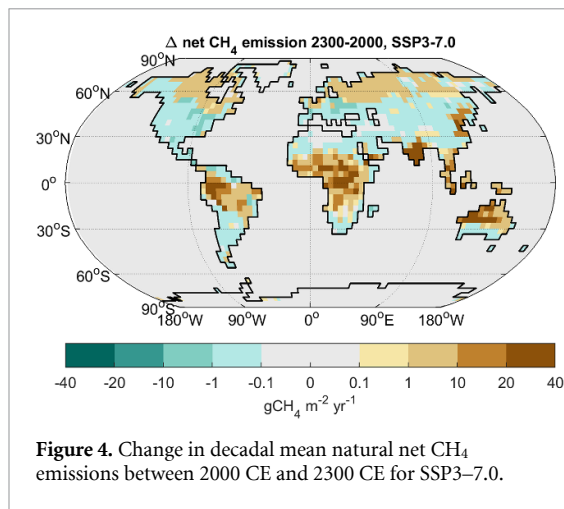


Figure 3. Anthropogenic methane emissions from Hoesly *et al* (2018) for the historical period, and from Gidden *et al* (2019) for the future. Emission scenarios end in 2100, therefore extended with a linear decrease of non-agricultural emissions to zero in 2250 CE, while agricultural emissions stay constant.

beyond 2100 CE in the scenarios with a radiative forcing larger than 2.6 Wm^{-2} .

In these scenario experiments, with the exception of SSP3–7.0, the natural emissions also become larger than the anthropogenic emissions (figure 3) and stay higher than at present for far longer than the anthropogenic emissions assumed in the scenarios (Gidden *et al* 2019, Meinshausen *et al* 2020). As a result, the atmospheric CH_4 concentrations will be higher—in the case of the large radiative forcing scenarios substantially higher—than in the published scenarios.

In the SSP3–7.0, as an example of a high radiative forcing scenario, global mean temperature increases rapidly by 6.8 K between 2010 CE and 2200 CE (figure A2), with the rate of increase diminishing after 2200 and temperature stabilising at a global mean warming of about 8.5 K after 2500 CE. The natural net methane emissions (figure 2) increase rapidly by 221% until 2200 CE, reach a maximum of $719 \text{ TgCH}_4 \text{ yr}^{-1}$ (+226%) in the 2310s, and decrease slowly thereafter, with emissions in 3000 CE still 2.6 times as large as in 2010. Anthropogenic emissions, for comparison, increase to $715 \text{ TgCH}_4 \text{ yr}^{-1}$ in 2100 CE and decline quickly thereafter (figure 3), until stabilising at $379 \text{ TgCH}_4 \text{ yr}^{-1}$ in 2250, as only agricultural emissions are assumed for anthropogenic emissions after this time. Spatially, the bulk of the increase in natural emissions (shown for 2300 CE) occurs in tropical regions (figure 4), with NH high latitudes



also showing significant increases, while net emissions from dryland regions decrease due to increasing soil uptake of CH₄. The developments in methane fluxes described for SSP3-7.0 are similar in the other two high radiative forcing scenarios, though with lower or higher absolute values for SSP2-4.5 and SSP5-8.5, respectively.

The other two scenarios, SSP1-1.9 and SSP1-2.6, are characterised by CO₂ concentrations which quickly decline after an initial peak (figure A1), leading to a substantially faster temperature decrease than in the other scenarios, with temperatures stabilising in the 22nd century. In SSP1-2.6, as an example of a low radiative forcing scenario, net CH₄ emissions increase to 299 TgCH₄ yr⁻¹ (+36% from 2010 CE) in the 2070s, then rapidly decline to 274 TgCH₄ yr⁻¹ in 2200 CE, followed by a gradual decrease to 256 TgCH₄ yr⁻¹ in 3000 CE. Being much smaller than the increase in the high warming scenarios, this nevertheless implies that natural methane emissions will exceed present-day fluxes by 15% or more throughout the next millennium and longer.

Concentrating on the time frame until 2200 CE, the phase of rapid increases in global mean temperature, the rise in natural net methane emissions is directly proportional to the change in global mean temperature with an emission increase by 75 TgCH₄ yr⁻¹ per K temperature increase (figure A4), independent of the chosen scenario. This temperature sensitivity of the natural net methane emissions leads to a sensitivity of the radiative forcing from methane of 0.1 Wm⁻² K⁻¹, based on Etminan *et al* (2016).

3.2. Wetland emissions

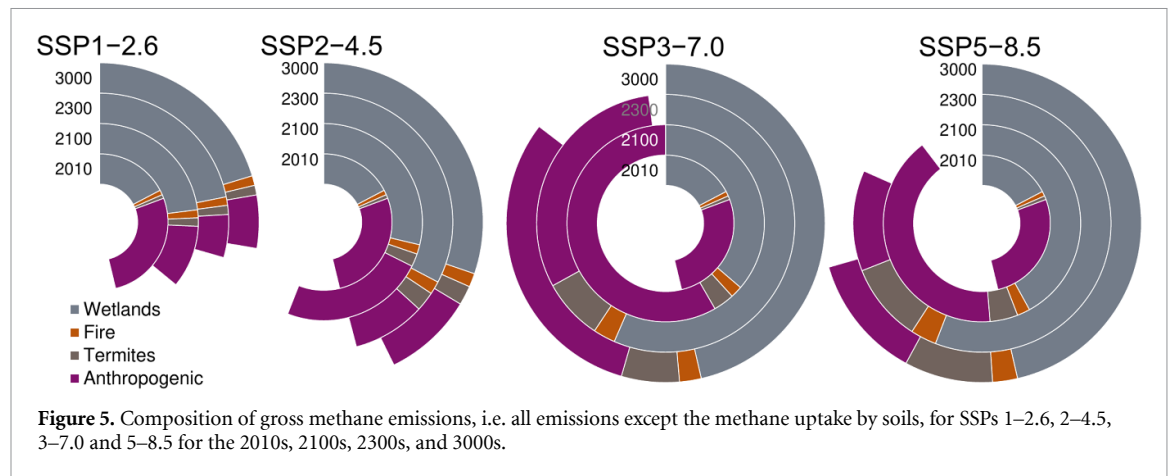
Wetland emissions are by far the largest component of the natural methane emissions in the present-day budget (Saunio *et al* 2020), with all other natural fluxes being of secondary importance. The bulk of wetland emissions (62%–77%) originates in the latitudes between 30°S and 30°N, while a much smaller part (20%–33%) is emitted from high latitudes

(Bousquet *et al* 2011). These relations do not change substantially under the SSP scenarios, with between 60% and 78% of the wetland emissions coming from low latitudes. For the wetland CH₄ emission change between last glacial maximum and preindustrial, we were able to show that the change can be explained by changes in atmospheric CO₂ concentration and soil carbon stocks, both contributing about 40% to the change, and the remaining 20% can be explained by further climate changes, with temperature and precipitation changes being most important (Kleinen *et al* 2020). We have no reason to assume that this relationship will not hold in future climate states, although the percentage shares of the contributions will likely be different. Looking at the high radiative forcing scenarios, a significant part of the emission increase in the low latitudes stems from expansion of wetland areas. This is different in high latitude areas, where winter freezing becomes less important as climate warms. As a result, the seasonality of inundation changes, although the annual maximum inundation does not change. Thus expanding wetland areas play a significant role in the low latitudes, but not in the boreal regions. However, the model version employed in our experiments does not explicitly consider permafrost and may therefore underestimate hydrological changes in present-day permafrost areas.

In the SSP3-7.0, wetland CH₄ emissions (figure A5) increase from 212 TgCH₄ yr⁻¹ in 2010 CE to 674 TgCH₄ yr⁻¹ in 2200 CE, reach a maximum of 699 TgCH₄ yr⁻¹ in the 2310s and slowly decrease afterwards, with emissions of 569 TgCH₄ yr⁻¹ in 3000 CE. The initial surging of wetland emissions is driven by a combination of an increase in vegetation productivity due to warming and CO₂ growth, warming-induced increase in soil carbon turnover, as well as an expansion of tropical wetland areas due to intensified precipitation. High latitude wetland areas, on the other hand, do not change in their maximum extent, although warmer winter conditions lead to larger effective (unfrozen) wetland areas in the winter season. The slow decrease in emissions after 2330 CE, on the other hand, is caused by a slow decline in the carbon available for anaerobic decomposition, as the enhanced turnover caused by warmer condition leads to a decline in the litter and soil carbon stocks. While wetland CH₄ emissions change in a very similar way in SSP2-4.5, the evolution in SSP5-8.5 is slightly different. Here, tropical wetland emissions decline more quickly for the first 150 years after the emission peak in the 2200s, due to a shift in precipitation patterns, leading to a drying in subtropical Africa and South-East Asia.

3.3. Other natural CH₄ sources and sinks

CH₄ emissions from termites in SSP3-7.0 increase from 11 TgCH₄ yr⁻¹ in 2010 CE to 88 TgCH₄ yr⁻¹ in 2200 CE, reach their maximum of 95 TgCH₄ yr⁻¹ in the 2280s, and slowly decrease to 74 TgCH₄ yr⁻¹ in



3000 CE. The initial rapid increase in termite methane emissions is very well correlated with the growth of CO₂ in the atmosphere, as tropical gross primary production (GPP) is the main driver of termite emissions in the model employed (Kirschke *et al* 2013, Saunio *et al* 2016), which is strongly influenced by atmospheric CO₂. Termite emissions become even larger in SSP5–8.5, where they increase to about 125 TgCH₄ yr⁻¹ in 2200 CE. As this flux appears to be rather large, we assume that the climate forcing in SSPs 3–7.0 and 5–8.5 exceeds the range of applicability of the model of termite emissions we are using (Kirschke *et al* 2013, Saunio *et al* 2016). However, we are not aware of any better approach to determine future termite methane emissions.

Methane emissions from fires (figure A7) in SSP3–7.0 increase from 14 TgCH₄ yr⁻¹ in 2010 CE to 33 TgCH₄ yr⁻¹ in 2200 CE, peaking at 35 TgCH₄ yr⁻¹ in the 2310s and decline to 27 TgCH₄ yr⁻¹ in 3000 CE. Even larger emissions (40 TgCH₄ yr⁻¹) are reached in SSP5–8.5, but nonetheless fires remain a small source of methane to the atmosphere.

Methane uptake in upland soils (figure A8) increases in SSP3–7.0 from 18 TgCH₄ yr⁻¹ in 2010 CE to 87 TgCH₄ yr⁻¹ in 2200 CE, peaking at 111 TgCH₄ yr⁻¹ in the 2360s. In our model this flux is largely determined by the gradient between the CH₄ concentrations in the atmosphere and in the soil, as all methane transported into upland soils is oxidised eventually, making the diffusive transport into the soil the limitation on the oxidation rate.

Climate warming will thus lead to a change in the composition of the gross methane emissions (figure 5): at present, anthropogenic emissions make up more than half the gross emission flux, but climate change will lead to a strong warming-induced increase in the natural emissions, which will eventually surpass the anthropogenic emissions. As a result, the anthropogenic emissions are only at present larger than the gross (i.e. without uptake) natural methane emissions. For the future, only the high anthropogenic methane emission scenario SSP3–7.0 shows larger anthropogenic than natural emissions for 2100,

while all other scenarios show that future natural emissions are larger than the anthropogenic ones.

3.4. Study limitations

Uncertainties in our study are high, and the exact numbers from our experiments will therefore have to be interpreted with caution. The experimental setup was not optimised for short-term climate change simulations over the historical (1850–2015) and near future (2016–2100) period, some of the rapidly changing forcings, such as land-use changes and aerosol emissions, were not taken into account. Historical (1850–2015) climate therefore is not reproduced as well as in some CMIP6 experiments. Qualitatively, however, we consider our experiment outcomes to be reliable: Our model shows strong increases in wetland methane emissions in comparison to the historical period, which are well explained by the combination of warming, CO₂ increase and increase in vegetation productivity.

Our modelled changes in wetland methane emissions show reasonable estimates for the LGM and PD states (Kleinen *et al* 2020). However, the modelled carbon cycle changes are dependent on both temperature and CO₂ changes. If the CO₂-fertilisation, the enhancement of vegetation productivity with rising CO₂, is overestimated in our model, this would also result in an overestimate of wetland CH₄ emission changes.

Termites and fires contribute substantially less to the natural methane emissions. Nonetheless the performance of the fire model has been validated for both historical and near future climate conditions (Lasslop *et al* 2014), giving confidence in those results. The strong increase in CH₄ emissions from termites displayed by our model for the high warming scenarios likely is an overestimate, however.

The atmospheric sink in our model was calibrated to consistently reproduce the observed LGM and present-day concentrations of methane, which also resulted in moderate variations in its atmospheric lifetime, in line with the recent findings on the present and glacial methane cycle (Naik *et al* 2013,

Murray *et al* 2014, Hopcroft *et al* 2017). Larger future changes in methane lifetime could affect the sensitivity of methane emissions to temperature in experiments similar to the ones shown here. However, the well-buffered atmospheric oxidative capacity, sustained to a large extent by compounds emitted from anthropogenic sources (foremost nitrogen oxides), renders such conditions unlikely until at least 2100 CE (Voulgarakis *et al* 2013, Lelieveld *et al* 2016). While we use a rather rigorous atmospheric CH₄ reactivity parameterisation, errors of up to 20% in the simulated CH₄ sink are admissible due to propagation of the uncertainties associated with the input parameters, viz. emissions of trace gases (such as NO_x and VOCs). The latter typically reach 50% even for the present-day conditions (Gromov *et al* 2017) and thus are the current limiting factor for CH₄ sink estimates. As a result, we are more confident in the simulated changes in natural methane emissions than in the projected atmospheric methane concentration.

We assume that ice sheets will not change under future climatic conditions. This assumption may be justified for the low warming scenarios, but it is clearly not justified for the high warming scenarios. It is highly unlikely that the Greenland ice sheet will remain unchanged for the next 1000 years if global mean temperature increases by 12 K. However, we do not have an interactive ice sheet model available at this time, and thus cannot evaluate the climatic consequences of the eventual waning of the Greenland (and likely West Antarctic) ice sheets.

Finally, the anthropogenic emission scenarios we are comparing to have only been published for the years until 2100 CE (Gidden *et al* 2019), and we are making the same assumptions as Meinshausen *et al* (2020) for the years beyond this time: we assume that agricultural emissions stay constant, and that the non-agricultural emissions decrease linearly until they reach zero in 2250 CE. This is an obvious simplification. However, no other extensions to the scenarios have been published yet, making it impossible for us to rely on other sources. Since all scenarios but SSP3–7.0 already have declining emissions in 2100 CE, we assume the error we are introducing for the non-agricultural emissions is not large. With regard to the agricultural emissions, it appears unlikely that they will stay constant indefinitely, and as population is declining by 2100 CE in all scenarios but SSP3–7.0 (KC and Lutz 2017), a decrease in agricultural emissions might be considered more logical. The anthropogenic emissions we are assuming for the years beyond 2100 CE therefore likely are an upper bound for all scenarios but SSP3–7.0.

4. Conclusions

Our results show that the natural CH₄ emissions will increase dramatically in high warming scenarios,

compared to the late historical period. This increase is predominantly driven by the increase in emissions from wetlands, caused by the combination of warmer temperatures, higher CO₂ concentrations leading to increased vegetation productivity, and changes in wetland seasonality or area. Furthermore, CH₄ emissions will remain larger than in the historical period for a long time, likely for as long as CO₂ and temperatures remain above present levels. As a result, atmospheric concentrations of methane are likely to be significantly higher than those obtained for CMIP6 with an assumption of constant natural emissions. The direct consequence is that radiative forcing from methane will be higher than assumed in the scenarios used in CMIP6—by 80% in the case of SSP3–7.0. This is a significant increase, although the forcing by methane is yet dwarfed by the forcing from CO₂.

Our results also bear on the recent discussion of the positive effects of short-term reductions in anthropogenic methane emissions (Ocko *et al* 2021): while a reduction in anthropogenic methane emissions will clearly be beneficial in reducing short-term climate warming, our results show that this effect will be short-lived, if CO₂ emissions are allowed to continue rising. In that case the natural methane emissions will increase in response to the warming and negate any positive effects of the reduction in anthropogenic methane emissions. A further consequence of the increased atmospheric methane concentration is a reduction of the atmospheric self-cleansing capacity via OH radicals, as additional OH is used up in the oxidation of methane. The resulting effects will impact removal of pollutants from the atmosphere, exacerbating negative health consequences and mortality, and increasing economic costs for air pollution control measures (Lelieveld *et al* 2015).

While the above-mentioned factors lead to some uncertainty about the exact increase in emissions (and atmospheric concentration) of CH₄, our main conclusions are robust, underlined by the fact that our model is able to reproduce methane changes from last glacial maximum to the present (Kleinen *et al* 2020). We thus conclude that the natural emissions of methane will increase much more strongly in response to warming than was assumed previously, becoming larger than the anthropogenic emissions in all scenarios investigated, with the exception of SSP3–7.0. This change needs to be taken into account when assessing future changes in atmospheric methane and radiative forcing.

Data availability statement

The data that support the findings of this study are openly available at the following URL/DOI: https://cera-www.dkrz.de/WDCC/ui/cersearch/entry?acronym=DKRZ_LTA_060_ds00007.

Acknowledgments

We acknowledge the World Climate Research Programme, which, through its Working Group on Coupled Modelling, coordinated and promoted CMIP6. We thank the authors of the CMIP6 input data sets for producing and making available these data, the Earth System Grid Federation (ESGF) for archiving the data and providing access, and the multiple funding agencies who support CMIP6 and ESGF.

We thank Goran Georgievski for comments on an earlier version of the paper. We acknowledge support through the project Palmod, funded by the German Federal Ministry of Education and Research (BMBF), Grant Nos. 01LP1921A and 01LP1921B. This work used resources of the Deutsches Klimarechenzentrum (DKRZ) granted by its Scientific Steering Committee (WLA) under Project ID bm1030.

Author contributions

T K: Methane emission model development, integration in MPIESM, design and execution of model experiments, main author of text. S G: Methane sink development, Methane lifetime analysis.

B S: Methane sink development, Methane lifetime analysis. V B: Experiment design, Scenario development. All: refinement of initial text.

Code and data availability

The primary data, i.e. the model code for MPI-ESM, are freely available to the scientific community and can be accessed with a license. In addition, secondary data and scripts that may be useful in reproducing the authors' work are archived by the Max Planck Institute for Meteorology. They can be obtained by contacting the first author or [http://publications@mpimet.mpg.de](mailto:publications@mpimet.mpg.de). Methane emission fields, as well as fields of near surface air temperature and precipitation, are publicly available from the World Data Center for Climate (WDCC) at DKRZ (Kleinen *et al* 2021), both as annual means for all years and as decadal climatologies of monthly means. The greenhouse gas trajectories used to drive the model experiments and the atmospheric methane concentration are also available there.

Conflict of interest

None.

Appendix. Extended figures

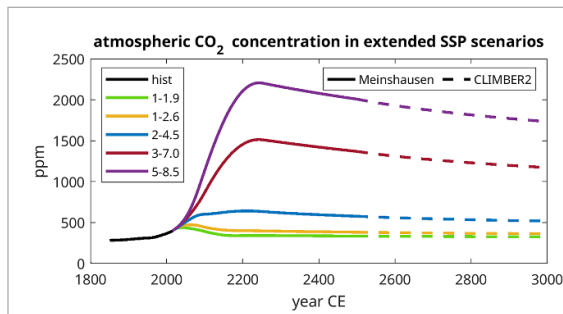


Figure A1. Atmospheric CO₂ concentration in extended SSP scenario experiments. Solid: as in Meinshausen et al (2020), dashed: scenario extension obtained with CLIMBER2 model.

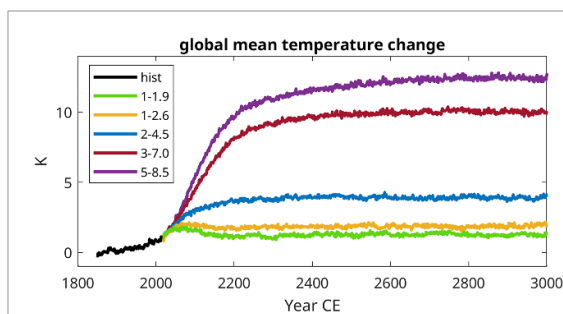


Figure A2. Change in global mean temperature, relative to 1850 CE, for historical period and scenario experiments.

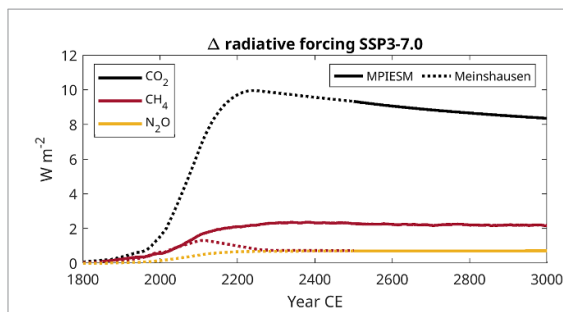


Figure A3. Radiative forcing change from preindustrial in SSP3-7.0, calculated after Etminan et al (2016). Dotted lines: Meinshausen et al (2020) scenarios, solid lines: MPIESM results (for CH₄) or scenario extension.

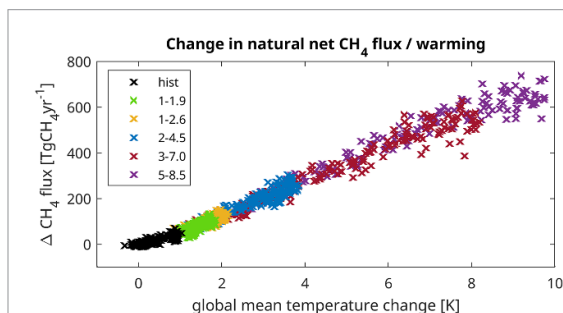


Figure A4. Change in natural net CH₄ flux, shown against global mean temperature change, for 1850–2200 CE. The relationship appears directly proportional with a slope of 75 TgCH₄ yr⁻¹ K⁻¹.

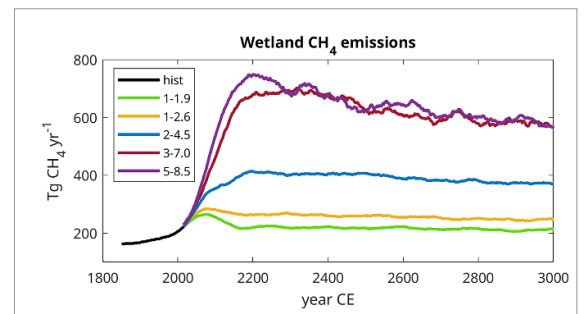


Figure A5. Wetland methane emissions in TgCH₄ yr⁻¹, 50-year running mean.

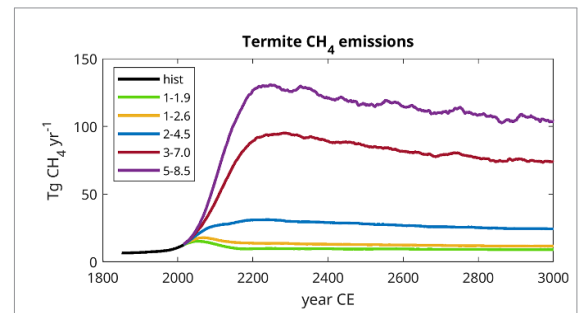


Figure A6. Termite methane emissions in TgCH₄ yr⁻¹, 50-year running mean.

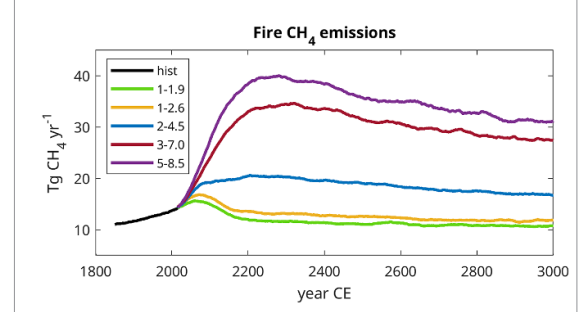


Figure A7. Methane emissions from fires in TgCH₄ yr⁻¹, 50-year running mean.

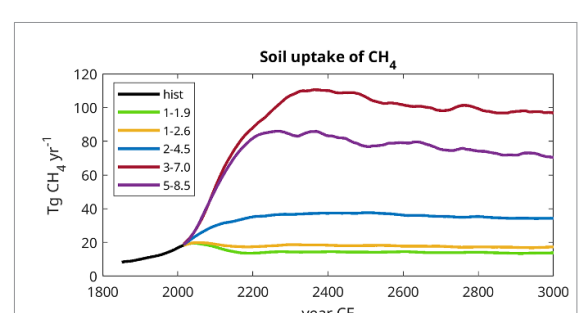


Figure A8. Soil uptake of methane in TgCH₄ yr⁻¹, 50-year running mean. Direction is reversed in comparison to other fluxes, as flux is into the soil.

ORCID iDs

Thomas Kleinen  <https://orcid.org/0000-0001-9550-5164>

Sergey Gromov  <https://orcid.org/0000-0002-2542-3005>

Benedikt Steil  <https://orcid.org/0000-0002-9750-3768>

Victor Brovkin  <https://orcid.org/0000-0001-6420-3198>

References

- Berger A L 1978 Long-term variations of daily insolation and quaternary climatic changes *J. Atmos. Sci.* **35** 2362–7
- Beven K J and Kirkby M J 1979 A physically based, variable contributing area model of basin hydrology *Hydrol. Sci. Bull.* **24** 43–69
- Bousquet P et al 2011 Source attribution of the changes in atmospheric methane for 2006–2008 *Atmos. Chem. Phys.* **11** 3689–700
- Briggs R D, Pollard D and Tarasov L 2014 A data-constrained large ensemble analysis of Antarctic evolution since the eemian *Quat. Sci. Rev.* **103** 91–115
- Brovkin V, Ganopolski A, Archer D and Munhoven G 2012 Glacial CO₂ cycle as a succession of key physical and biogeochemical processes *Clim. Past* **8** 251–64
- Ciais P et al 2013 Carbon and other biogeochemical cycles *Climate Change 2013: The Physical Science Basis. Contribution of Working Group I to the Fifth Assessment Report of the Intergovernmental Panel on Climate Change* ed T Stocker et al (Cambridge: Cambridge University Press) ch 6, pp 465–570
- Dean J F et al 2018 Methane feedbacks to the global climate system in a warmer world *Rev. Geophys.* **56** 207–50
- Denisov S N, Eliseev A V and Mokhov I I 2013 Climate change in IAP RAS global model taking account of interaction with methane cycle under anthropogenic scenarios of RCP family *Russ. Meteorol. Hydrol.* **38** 741–9
- Etiopie G 2015 *Gas Seepage Classification and Global Distribution* (Cham: Springer International Publishing) pp 17–43
- Etminan M, Myhre G, Highwood E J and Shine K P 2016 Radiative forcing of carbon dioxide, methane and nitrous oxide: a significant revision of the methane radiative forcing *Geophys. Res. Lett.* **43** 12614–23
- Friedlingstein P et al 2019 Global carbon budget 2019 *Earth Syst. Sci. Data* **11** 1783–838
- Gidden M et al 2018a *input4MIPs.CMIP6. ScenarioMIP.IAMC.IAMC-IMAGE-ssp119-1-1* version 20180620 (available at: <https://doi.org/10.22033/ESGF/input4MIPs.2485>)
- Gidden M et al 2018b *input4MIPs.CMIP6. ScenarioMIP.IAMC.IAMC-IMAGE-ssp126-1-1* version 20180620 (available at: <https://doi.org/10.22033/ESGF/input4MIPs.2486>)
- Gidden M et al 2018c *input4MIPs.CMIP6. ScenarioMIP.IAMC.IAMC-MESSAGE-GLOBIOM-ssp245-1-1* version 20180620 (available at: <https://doi.org/10.22033/ESGF/input4MIPs.2487>)
- Gidden M et al 2018d *input4MIPs.CMIP6. ScenarioMIP.IAMC.IAMC-AIM-ssp370-1-1* version 20180620 (available at: <https://doi.org/10.22033/ESGF/input4MIPs.2482>)
- Gidden M et al 2018e *input4MIPs.CMIP6. ScenarioMIP.IAMC.IAMC-REMIND-MAGPIE-ssp585-1-1* version 20180620 (available at: <https://doi.org/10.22033/ESGF/input4MIPs.2489>)
- Gidden M J et al 2019 Global emissions pathways under different socioeconomic scenarios for use in CMIP6: a dataset of harmonized emissions trajectories through the end of the century *Geosci. Model Dev.* **12** 1443–75
- Goll D S, Brovkin V, Liski J, Raddatz T, Thum T and Todd-Brown K E O 2015 Strong dependence of CO₂ emissions from anthropogenic land cover change on initial land cover and soil carbon parametrization *Glob. Biogeochem. Cycles* **29** 1511–23
- Grewe V, Brunner D, Dameris M, Grenfell J, Hein R, Shindell D and Staehelin J 2001 Origin and variability of upper tropospheric nitrogen oxides and ozone at northern mid-latitudes *Atmos. Environ.* **35** 3421–33
- Gromov S, Brenninkmeijer C A M and Jöckel P 2017 Uncertainties of fluxes and ¹³C/¹²C ratios of atmospheric reactive-gas emissions *Atmos. Chem. Phys.* **17** 8525–52
- Gromov S, Steil B, Kleinen T and Brovkin V 2018 On the factors controlling the atmospheric oxidative capacity and CH₄ lifetime during the LGM *Geophys. Res. Abstr.* **20** 19038
- Guenther A B, Jiang X, Heald C L, Sakulyanontvittaya T, Duhl T, Emmons L K and Wang X 2012 The model of emissions of gases and aerosols from nature version 2.1 (MEGAN2.1): an extended and updated framework for modeling biogenic emissions *Geosci. Model Dev.* **5** 1471–92
- Hmiel B et al 2020 Preindustrial ¹⁴CH₄ indicates greater anthropogenic fossil CH₄ emissions *Nature* **578** 409–12
- Hoesly R et al 2017a *Historical Emissions (1750–2014)—CEDS—v2017-05-18* version 20170519 (available at: <https://doi.org/10.22033/ESGF/input4MIPs.1241>)
- Hoesly R et al 2017b *Supplemental Historical Emissions (1750–2014)—CEDS—v2017-05-18* version 20170711 (available at: <https://doi.org/10.22033/ESGF/input4MIPs.1242>)
- Hoesly R M et al 2018 Historical (1750–2014) anthropogenic emissions of reactive gases and aerosols from the community emissions data system (CEDS) *Geosci. Model Dev.* **11** 369–408
- Hopcroft P O, Valdes P J, O'Connor F M, Kaplan J O and Beerling D J 2017 Understanding the glacial methane cycle *Nat. Commun.* **8** 14383
- Ivanovic R E, Gregoire L J, Kageyama M, Roche D M, Valdes P J, Burke A, Drummond R, Peltier W R and Tarasov L 2016 Transient climate simulations of the deglaciation 21–9 thousand years before present (version 1)—PMIP4 core experiment design and boundary conditions *Geosci. Model Dev.* **9** 2563–87
- Joekel P, Kerkweg A, Pozzer A, Sander R, Tost H, Riede H, Baumgaertner A, Gromov S and Kern B 2010 Development cycle 2 of the modular earth submodel system (MESSy2) *Geosci. Model Dev.* **3** 717–52
- Kaiser J W et al 2012 Biomass burning emissions estimated with a global fire assimilation system based on observed fire radiative power *Biogeosciences* **9** 527–54
- KC S and Lutz W 2017 The human core of the shared socioeconomic pathways: population scenarios by age, sex and level of education for all countries to 2100 *Glob. Environ. Change* **42** 181–92
- Kirschke S et al 2013 Three decades of global methane sources and sinks *Nat. Geosci.* **6** 813–23
- Kleinen T, Brovkin V and Munhoven G 2016 Modelled interglacial carbon cycle dynamics during the holocene, the eemian and marine isotope stage (MIS) 11 *Clim. Past* **12** 2145–60
- Kleinen T, Mikolajewicz U and Brovkin V 2020 Terrestrial methane emissions from the last glacial maximum to the preindustrial period *Clim. Past* **16** 575–95
- Kleinen T, Gromov S, Steil B, and Brovkin V 2021 *Natural Methane Emissions 1850–3009* (available at: http://cera-www.dkrz.de/WDCC/ui/Compact.jsp?acronym=DKRZ_LTA_1030_ds00001)
- Koffi E N, Bergamaschi P, Alkama R and Cescatti A 2020 An observation-constrained assessment of the climate sensitivity and future trajectories of wetland methane emissions *Sci. Adv.* **6** eaay4444
- Köhler P, Nehrass-Ahles C, Schmitt J, Stocker T F and Fischer H 2017 A 156 kyr smoothed history of the atmospheric

- greenhouse gases CO₂, CH₄ and N₂O and their radiative forcing *Earth Syst. Sci. Data* **9** 363–87
- Lasslop G, Thonicke K and Kloster S 2014 SPITFIRE within the MPI earth system model: model development and evaluation *J. Adv. Model. Earth Syst.* **6** 740–55
- Lelieveld J, Evans J S, Fnais M, Giannadaki D and Pozzer A 2015 The contribution of outdoor air pollution sources to premature mortality on a global scale *Nature* **525** 367–71
- Lelieveld J, Gromov S, Pozzer A and Taraborrelli D 2016 Global tropospheric hydroxyl distribution, budget and reactivity *Atmos. Chem. Phys.* **16** 12477–93
- Mauritsen T et al 2019 Developments in the MPI-M earth system model version 1.2 (MPI-ESM1.2) and its response to increasing CO₂ *J. Adv. Model. Earth Syst.* **11** 998–1038
- Meinshausen M and Nicholls Z R J 2018a *UoM-IMAGE-ssp119-1-2-1 GHG concentrations* (available at: <https://doi.org/10.22033/ESGF/input4MIPs.9864>)
- Meinshausen M and Nicholls Z R J 2018b *UoM-IMAGE-ssp126-1-2-1 GHG concentrations* (available at: <https://doi.org/10.22033/ESGF/input4MIPs.9865>)
- Meinshausen M and Nicholls Z R J 2018c *UoM-MESSAGE-GLOBIOM-ssp245-1-2-1 GHG concentrations* (available at: <https://doi.org/10.22033/ESGF/input4MIPs.9866>)
- Meinshausen M and Nicholls Z R J 2018d *UoM-AIM-ssp370-1-2-1 GHG concentrations* (available at: <https://doi.org/10.22033/ESGF/input4MIPs.9861>)
- Meinshausen M and Nicholls Z R J 2018e *UoM-REMIND-MAGPIE-ssp585-1-2-1 GHG concentrations* (available at: <https://doi.org/10.22033/ESGF/input4MIPs.9868>)
- Meinshausen M and Vogel E 2016 *input4MIPs.UoM.GHGConcentrations.CMIP.UoM-CMIP-1-2-0 version 20160830* (available at: <https://doi.org/10.22033/ESGF/input4MIPs.1118>)
- Meinshausen M, Raper S C B and Wigley T M L 2011 Emulating coupled atmosphere-ocean and carbon cycle models with a simpler model, MAGICC6—part 1: model description and calibration *Atmos. Chem. Phys.* **11** 1417–56
- Meinshausen M et al 2020 The shared socio-economic pathway (SSP) greenhouse gas concentrations and their extensions to 2500 *Geosci. Model Dev.* **13** 3571–605
- Mikolajewicz U et al 2018 The climate of a retrograde rotating earth *Earth Syst. Dyn.* **9** 1191–1215
- Murray L T, Mickley L J, Kaplan J O, Sofen E D, Pfeiffer M and Alexander B 2014 Factors controlling variability in the oxidative capacity of the troposphere since the last glacial maximum *Atmos. Chem. Phys.* **14** 3589–622
- Myhre G et al 2013 Anthropogenic and natural radiative forcing *Climate Change 2013: The Physical Science Basis. Contribution of Working Group I to the Fifth Assessment Report of the Intergovernmental Panel on Climate Change* ed T Stocker et al (Cambridge: Cambridge University Press) ch 8, pp 659–740
- Naik V et al 2013 Preindustrial to present-day changes in tropospheric hydroxyl radical and methane lifetime from the atmospheric chemistry and climate model intercomparison project (ACCMIP) *Atmos. Chem. Phys.* **13** 5277–98
- Ocko I B, Sun T, Shindell D, Oppenheimer M, Hristov A N, Pacala S W, Mauzerall D L, Xu Y and Hamburg S P 2021 Acting rapidly to deploy readily available methane mitigation measures by sector can immediately slow global warming *Environ. Res. Lett.* **16** 054042
- O'Neill B C et al 2016 The scenario model intercomparison project (ScenarioMIP) for CMIP6 *Geosci. Model Dev.* **9** 3461–82
- Prigent C, Papa F, Aires F, Jimenez C, Rossow W B and Matthews E 2012 Changes in land surface water dynamics since the 1990s and relation to population pressure *Geophys. Res. Lett.* **39** L08403
- Riley W J, Subin Z M, Lawrence D M, Swenson S C, Torn M S, Meng L, Mahowald N M and Hess P 2011 Barriers to predicting changes in global terrestrial methane fluxes: analyses using CLM4Me, a methane biogeochemistry model integrated in CESM *Biogeosciences* **8** 1925–53
- Saunio M et al 2016 The global methane budget 2000–2012 *Earth Syst. Sci. Data* **8** 697–751
- Saunio M et al 2020 The global methane budget 2000–2017 *Earth Syst. Sci. Data* **12** 1561–623
- Shindell D T et al 2013 Interactive ozone and methane chemistry in GISS-E2 historical and future climate simulations *Atmos. Chem. Phys.* **13** 2653–89
- Tarasov L, Dyke A S, Neal R M and Peltier W 2012 A data-calibrated distribution of deglacial chronologies for the north american ice complex from glaciological modeling *Earth Planet. Sci. Lett.* **315–316** 30–40
- van Groenigen K J, Osenberg C W and Hungate B A 2011 Increased soil emissions of potent greenhouse gases under increased atmospheric CO₂ *Nature* **475** 214–16
- Voulgarakis A et al 2013 Analysis of present day and future OH and methane lifetime in the ACCMIP simulations *Atmos. Chem. Phys.* **13** 2563–87
- Wania R, Ross I and Prentice I C 2010 Implementation and evaluation of a new methane model within a dynamic global vegetation model: LPJ-WHyMe v1.3.1 *Geosci. Model Dev.* **3** 565–84
- Zhang Z, Zimmermann N E, Stenke A, Li X, Hodson E L, Zhu G, Huang C and Poulter B 2017 Emerging role of wetland methane emissions in driving 21st century climate change *Proc. Natl Acad. Sci.* **114** 9647–52